Mycobacterium tuberculosis DNA repair helicase UvrD1 is activated by redox-dependent dimerization via a 2B domain cysteine

Ankita Chadda[a], Drake Jensen[a], Eric J. Tomko[a], Ana Ruiz Manzano[a], Binh Nguyen[a], Timothy M. Lohman[a], and Eric A. Galburt[a,1]

[a]Department of Biochemistry and Molecular Biophysics, Washington University in Saint Louis, Saint Louis, MO 63110

Edited by Mark Dillingham, Department of Biochemistry, Bristol University, Bristol, United Kingdom; received August 6, 2021; accepted December 31, 2021, by Editorial Board Member Kiyoshi Mizuuchi

***Mycobacterium tuberculosis* (*Mtb*) causes tuberculosis and, during infection, is exposed to reactive oxygen species and reactive nitrogen intermediates from the host immune response that can cause DNA damage. UvrD-like proteins are involved in DNA repair and replication and belong to the SF1 family of DNA helicases that use ATP hydrolysis to catalyze DNA unwinding. In *Mtb*, there are two UvrD-like enzymes, where UvrD1 is most closely related to other family members. Previous studies have suggested that UvrD1 is exclusively monomeric; however, it is well known that *Escherichia coli* UvrD and other UvrD family members exhibit monomer–dimer equilibria and unwind as dimers in the absence of accessory factors. Here, we reconcile these incongruent studies by showing that *Mtb* UvrD1 exists in monomer, dimer, and higher-order oligomeric forms, where dimerization is regulated by redox potential. We identify a 2B domain cysteine, conserved in many Actinobacteria, that underlies this effect. We also show that UvrD1 DNA-unwinding activity correlates specifically with the dimer population and is thus titrated directly via increasing positive (i.e., oxidative) redox potential. Consistent with the regulatory role of the 2B domain and the dimerization-based activation of DNA unwinding in UvrD family helicases, these results suggest that UvrD1 is activated under oxidizing conditions when it may be needed to respond to DNA damage during infection.**

DNA helicase | *Mycobacterium tuberculosis* | UvrD | redox potential | DNA repair

DNA repair plays an essential role in the ability of organisms to maintain genome integrity in the face of environmental stresses. One particularly flexible and conserved pathway is nucleotide excision repair (NER), which detects and repairs bulky nucleotide lesions caused by ultraviolet (UV) light, environmental mutagens, and a subset of oxidative lesions (1–3). In bacteria, global genome NER is initiated when lesions are recognized directly by UvrA, although an alternative pathway called transcription-coupled NER depends on RNA polymerase stalling as the initiation event (4–7). The removal of the lesion eventually requires the recruitment of a helicase to the site of damage. In eukaryotes, this function is filled by the general transcription factor IIH (TFIIH) (8–10), while prokaryotes utilize the UvrD-family enzymes (1, 3, 11). In addition to its role in NER, UvrD participates in a range of other pathways of DNA metabolism, such as replication (12–15) and recombination (16–18).

UvrD has been well characterized in many contexts and from model organisms, including *Escherichia coli* and *Bacillus subtilis*. It is a superfamily 1A (SF1A) helicase, as defined by core helicase domains 1A and 1B coupled with auxiliary 2A and 2B subdomains (19, 20). It can both translocate on single-stranded DNA (ssDNA) and unwind double-stranded DNA (dsDNA) under specific conditions. More precisely, while monomers of UvrD family members (UvrD, Rep, and PcrA) are ATP-dependent ssDNA translocases, dimeric forms of these enzymes are required to unwind duplex DNA in vitro in the absence of accessory factors or force (21–27). In Rep, this activation is regulated by the mobile 2B domain, as both deletion of the 2B domain or a cross-linked 2B domain construct activate the Rep monomer for unwinding (28, 29). Activation of the dimeric UvrD helicase is also accompanied by reorientation of its 2B subdomain (30). Additionally, the rotational orientation of the 2B domain regulates the force-dependent unwinding activity of both UvrD and Rep monomers (31, 32). Helicase activation can also occur via binding with accessory factors. For example, *B. stearothermophilus* RepD activates PcrA monomers (25, 31, 32), and the mismatch repair protein MutL activates UvrD monomers (33, 34). Furthermore, these interactions directly affect the orientation of the regulatory 2B domain (34). In addition to its association with other repair proteins (32), UvrD associates with RNA polymerase through its C-terminal RNA polymerase (RNAP) interaction domain (RID) during one mode of transcription-coupled NER (35–37). This interaction leads to the stimulation of RNAP backtracking and the recruitment of UvrAB (37).

While many studies have been reported focusing on UvrD family helicases from model bacteria, less is known about these enzymes in the distantly related human pathogen *Mycobacterium tuberculosis* (*Mtb*). *Mtb* is the causative agent of tuberculosis and is the leading cause of death worldwide from an

Significance

***Mycobacterium tuberculosis* (*Mtb*) is an intracellular pathogen that causes tuberculosis and is exposed to oxidative insults from immune system macrophages. *Mtb* UvrD1 plays a role in DNA repair during infection and has been suggested to function as a monomer. However, we find that UvrD1 can self-assemble, the balance between monomer and dimer depends on redox potential via a cysteine residue in the regulatory 2B domain, and unwinding activity is uniquely a property of the dimer. Our results provide direct evidence of the domain interface in these ubiquitous enzymes, reveal a subfamily of UvrD-like enzymes regulated by redox potential, and suggest that *Mtb* UvrD1 is activated by the oxidative conditions imposed during infection.**

Author contributions: A.C., T.M.L., and E.A.G. designed research; A.C. performed research; A.R.M. and B.N. contributed new reagents/analytic tools; A.C., D.J., E.J.T., B.N., T.M.L., and E.A.G. analyzed data; and A.C., T.M.L., and E.A.G. wrote the paper.

The authors declare no competing interest.

This article is a PNAS Direct Submission. M.D. is a guest editor invited by the Editorial Board.

This article is distributed under Creative Commons Attribution-NonCommercial-NoDerivatives License 4.0 (CC BY-NC-ND).

[1]To whom correspondence may be addressed. Email: egalburt@wustl.edu.

This article contains supporting information online at http://www.pnas.org/lookup/suppl/doi:10.1073/pnas.2114501119/-/DCSupplemental.

Published February 16, 2022.

Downloaded at SCHL MED LIB&77680003 on February 16, 2022

BIOCHEMISTRY

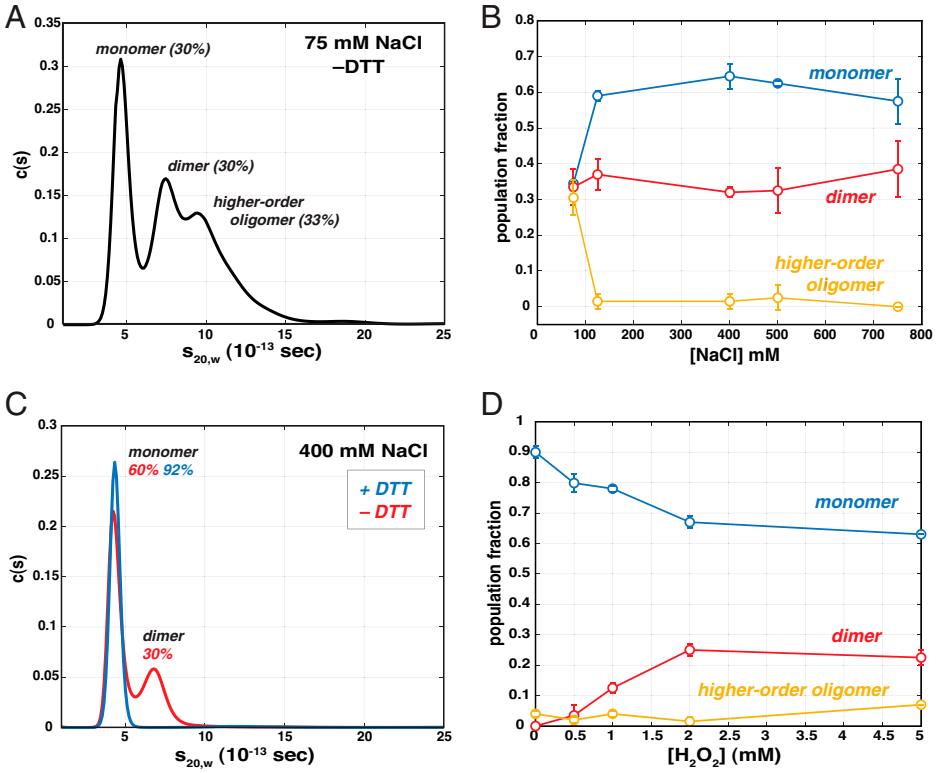

Fig. 1. Oligomeric states of UvrD1. (*A*) Sedimentation velocity trace measured at 230 nm in Buffer A plus 75 mM NaCl in the absence of DTT reveals the presence of monomeric, dimeric, and higher-order oligomeric species. (*B*) Summary of results from AUC velocity experiments using 2.5 μM UvrD1 in the absence of DTT as a function of NaCl concentration (*SI Appendix*, Fig. S3). From 75 mM to 750 mM NaCl, the fraction of monomer present in the monomeric state (blue), dimeric state (red), and higher-order oligomeric states (yellow) are shown. (*C*) The continuous distribution of species from AUC velocity runs measured at 280 nm with 400 mM NaCl in the presence and absence of 1 mM DTT. (*D*) After treatment of 2.5 μM WT UvrD1 in 75 mM NaCl with 1 mM DTT, a titration series of H_2O_2 from 0 mM to 5 mM was run in AUC velocity experiments (*SI Appendix*, Fig. S5). Increasing concentrations of H_2O_2 result in a decrease in the fraction found in the monomeric state (blue) and an increasing fraction found in the dimeric state (red). Higher-order oligomeric states (yellow) represented less than 10% under all conditions.

infectious agent (38). Although DNA metabolism pathways, such as transcription and repair, are generally conserved in bacteria, important differences exist (39–42). This appears to be especially true in *Mtb*, perhaps as it is highly evolved for a relatively narrow niche (43). Interestingly, and in contrast to model bacteria, *Mtb* contains two UvrD family enzymes: UvrD1 and UvrD2 (44, 45). UvrD1 has high homology to *E. coli* UvrD, including the C-terminal RID (45, 46). Previous work on *Mtb* UvrD1 has shown that it is important for survival after UV and oxidative damage as well as for pathogenesis in mice (47). In stark contrast to other UvrD family members, UvrD1 has been reported to be monomeric and to either possess helicase activity directly or require activation via the binding of *Mtb* Ku (45, 46, 48).

Here, we report that UvrD1 exists in monomer, dimer, and higher-order oligomeric forms, where dimerization is redox dependent and is correlated with helicase activity. We identify a 2B domain cysteine that is required for the redox-dependent dimerization, demonstrating that the 2B subdomain is directly involved in dimerization. Our results explain the function of UvrD1 in the context of the large body of work on UvrD family proteins and suggest a model where UvrD1 senses the oxidative conditions within human macrophages during infection through dimerization, resulting in activation of its DNA-unwinding activity needed for DNA repair and other DNA metabolic pathways (49–51).

Results

The Oligomeric State of UvrD1 Is Redox Dependent. Previous studies reported that UvrD1 exists exclusively as a monomer in solution (45, 48). However, upon purifying UvrD1 as described in *Materials and Methods*, we observed two elution peaks from an S300 size-exclusion column run at 4 °C in Tris, pH 8.0, at 25 °C, 150 mM NaCl, and 10% glycerol and no dithiothreitol (DTT), consistent with the molecular weights of both monomer (85-kDa) and dimer (170-kDa) species (*SI Appendix*, Fig. S1). This result is consistent with studies of *E. coli* UvrD, which exhibits a monomer–dimer higher-order oligomer equilibrium (23, 26). To examine this more quantitatively, we performed analytical ultracentrifugation sedimentation velocity experiments in Tris, pH 8.0, at 25 °C and 20% glycerol (from here on defined as Buffer A) with 75 mM NaCl and 2.5 μM UvrD1. The continuous sedimentation coefficient ($c[s]$) distribution (52) shows three peaks that we assign to be monomer, dimer, and higher-order oligomers (Fig. 1*A* and *SI Appendix*, Table S1). The positions of the peaks do not change with UvrD1 concentration, indicating that each peak represents a single species; however, the amplitudes of the three peaks change with UvrD1 concentration as expected for a self-assembling monomer–dimer oligomer system (*SI Appendix*, Fig. S2). The oligomeric states of *E. coli* UvrD depend on the salt and glycerol concentrations, with the monomer population favored by higher salt and glycerol concentrations (26). We examined the salt dependence of the UvrD1 oligomeric state by sedimentation velocity at 2.5 μM UvrD1 in a range of NaCl concentrations between 75 and 750 mM. Surprisingly, the ratio of monomer to dimer was relatively constant throughout the salt titration apart from the lowest salt concentrations, where higher-order oligomers were populated at the expense of the monomer population (Fig. 1*B* and *SI Appendix*, Fig. S3).

Downloaded at SCHL MED LIB&77680003 on February 16, 2022

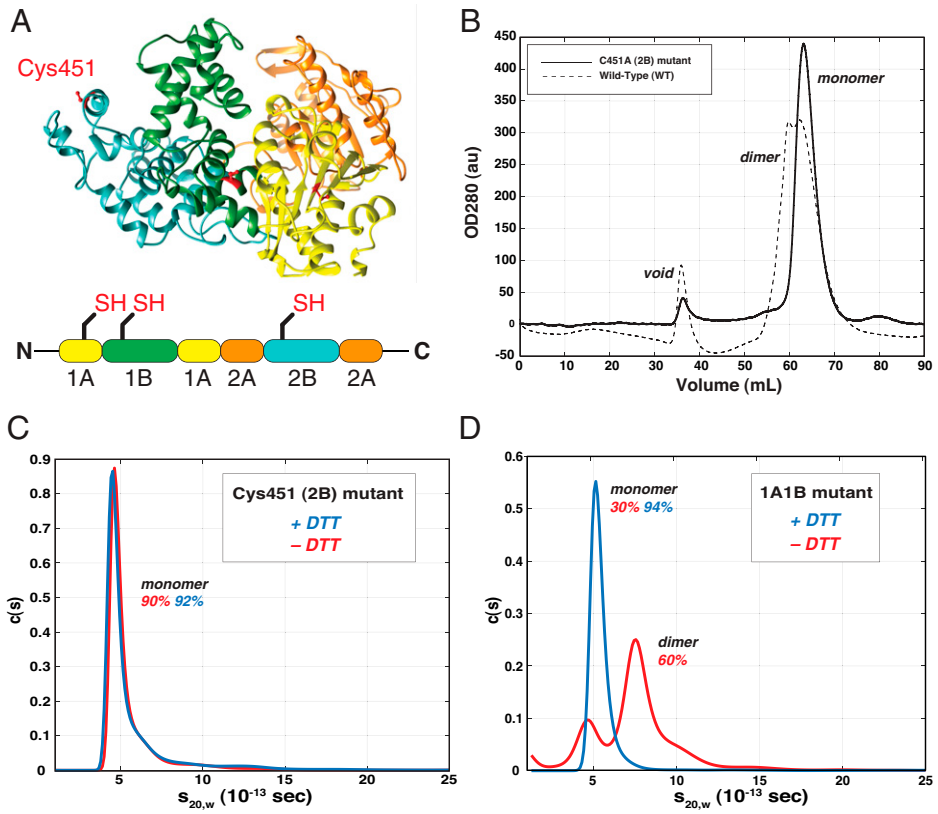

Fig. 2. Redox dependence of UvrD1 dimerization is due to C451 in the 2B domain. (*A*) Predicted structure of UvrD1 from threading UvrD1 sequence on the *E. coli* UvrD structure (PDB: 3LFU). Domain organization is indicated as well as the position of the three cysteine residues described in the text. (*B*) SEC (S300) of C451A mutant (solid) compared to WT (dashed). Both constructs were run in Tris, pH 8.0, 150 mM NaCl, and 10% glycerol and the absence of DTT as in *SI Appendix*, Fig. S1. (*C*) AUC velocity experiments on the 2B mutant in Buffer A plus 75 mM NaCl and the presence (blue) and absence (red) of DTT indicate that the mutant loses the ability to dimerize. Each trace is an average of two runs, and the population fractions for monomer and dimer are indicated. (*D*) In contrast, AUC velocity of the 1A1B double mutant in 75 mM NaCl and the presence (blue) and absence (red) of 1 mM DTT indicate that this mutant retains and even enhances dimer formation. Each trace is an average of two runs, and population fractions for monomer and dimer are indicated.

In contrast, the addition of 1 mM DTT at 400 mM NaCl in Buffer A shifted the species fraction dramatically to favor the monomer (96%; Fig. 1*C*). Even at the lowest NaCl concentration of 75 mM NaCl, the addition of 1 mM DTT resulted in a nearly uniform monomer population (90%; *SI Appendix*, Fig. S4). Thus, we hypothesized that UvrD1 dimerization is dependent on redox potential and reasoned that oxidative conditions should favor dimer formation just as reductive conditions favor the monomer species. To test this, we performed sedimentation velocity experiments in the presence of oxidizing agents after reduction by 1 mM DTT. As predicted, titration of hydrogen peroxide (H_2O_2) resulted in an increase in the dimer population (Fig. 1*D* and *SI Appendix*, Fig. S5). At 2 mM H_2O_2, the population fraction of dimer saturated at ~25%, and the addition of more H_2O_2 did not lead to more dimer formation.

A 2B Domain–2B Domain Disulfide Bond Is Responsible for Redox-Dependent Dimerization of UvrD1. The dependence of oligomerization on oxidation suggested a role for a thiol-containing amino acids, such as methionine or cysteine. In particular, we considered that the potential of cysteines to form disulfide bonds could lead to the formation of dimeric and higher-order oligomers. UvrD1 has three cysteine residues for which we estimated their approximate position by generating a threaded homology model of UvrD1 based on the structure of *E. coli* UvrD (Protein Data Bank [PDB]: 3LFU, PHYRE2; *Materials and Methods* and Fig. 2*A*). This model shows that while two cysteines appear buried within the 1A and 1B domains (C107 and C269), a third cysteine (C451) is surface exposed within the 2B domain. Surface calculations of our model with Chimera (53) confirmed this, as only C451 possesses solvent-exposed surface area in both open (based on the *E. coli* PDB 3LFU structure) and closed (based on the *Geobacillus stearothermophilus* PDB 3PJR structure) conformations (*SI Appendix*, Fig. S6). We hypothesized that a disulfide bond between the 2B cysteines of two monomers was responsible for the redox-dependent dimerization. To test this, we constructed and purified a C451A mutant (which we will refer to as the 2B mutant) and examined whether it is able to form dimers. During purification of this construct, the S300 elution profile showed only a single peak consistent with a monomer in contrast to wild-type (WT) UvrD1 (Fig. 2*B*). Sedimentation velocity experiments confirmed this result, as the 2B cysteine mutant was monomeric in both the presence and absence of DTT (Fig. 2*C* and *SI Appendix*, Table S1). In contrast, a double mutant of the 1A and 1B domain cysteines (C107T/C269T, now referred to as the 1A1B double mutant) maintained the ability to form dimers (Fig. 2*D* and *SI Appendix*, Table S1).

The three cysteine residues found in UvrD1 are not conserved in *E. coli* UvrD, despite the presence of six cysteine residues (Fig. 3*A*), and *E. coli* UvrD does not display a redox-dependent dimerization (*SI Appendix*, Fig. S7). However, the 2B domain cysteine identified here is conserved across various Actinobacterial classes (Fig. 3 *B* and *C* and *SI Appendix*, Fig. S8). A particularly high, but not universal, conservation was found in the Corynebacteriales order, which includes *Mtb* and other pathogenic bacteria (54, 55). In addition, we found the same sequence in the PcrA

Downloaded at SCHL MED LIB&77680003 on February 16, 2022

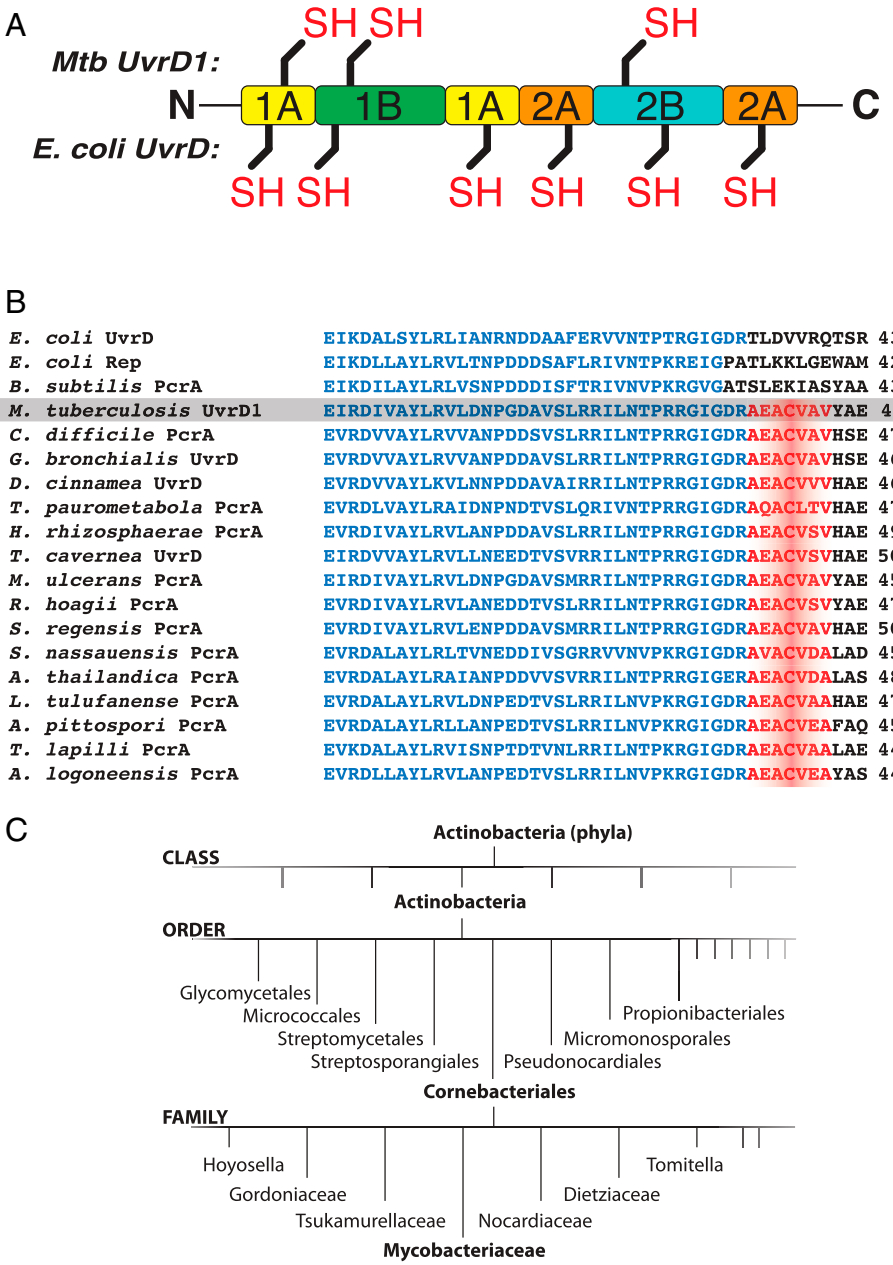

Fig. 3. Sequence distribution across bacterial species. (*A*) Distribution of cysteine residues in *Mtb* UvrD1 compared to *E. coli* UvrD. (*B*) Sequence alignment of the 2B domain region containing C451. The blue sequence is conserved across all UvrD-like family members, while the sequence containing the 2B cysteine residue (red) is distinct from *E. coli* and *B. subtilis* UvrD-family enzymes but conserved in many Actinomycetes. See *SI Appendix* for full species names. (*C*) Orders and families of Actinobacteria where the 2B cysteine can be found in available sequence data.

helicase found in one strain of the Firmicute *Clostridioides difficile* (NCTC13750), which represents another important human pathogen that interacts with macrophages (56, 57).

The Dimer of UvrD1 Is Required for DNA-Unwinding Activity. Previous studies of UvrD1 suggested that the monomer possesses helicase activity (48). However, this conclusion was based on measurements of helicase activity performed under solution conditions distinct from those used to examine its oligomerization state. In particular, the analysis of oligomeric state was performed in the presence of 5 mM DTT, while helicase assays were performed in buffer lacking DTT entirely (48). In other studies, UvrD1 was surmised to be a monomer based on sedimentation through a glycerol gradient and was reported to have feeble unwinding activity that was dramatically activated in the presence of *Mtb* Ku (45).

Given the observations of other UvrD family helicases (23, 25, 26, 28, 58), we hypothesized that only the dimer of UvrD1 would be capable of unwinding DNA. To test this hypothesis, we used a stopped-flow assay to measure the time dependence of UvrD1-catalyzed DNA unwinding (Fig. 4*A*). Specifically, we used a double-stranded 18-base pair (bp) DNA with a single-stranded dT_{20} 3′-flanking region (tail) with a Cy5 fluorophore on the 5′-end of the tailed strand and a black hole quencher (BHQ2) on the 3′-end of the complementary strand, as described previously (33, 34). In the double-stranded form, fluorescence from Cy5 is quenched due to the presence of the BHQ2 (59). Upon full unwinding, the strands are separated,

Downloaded at SCHL MED LIB&77880003 on February 16, 2022

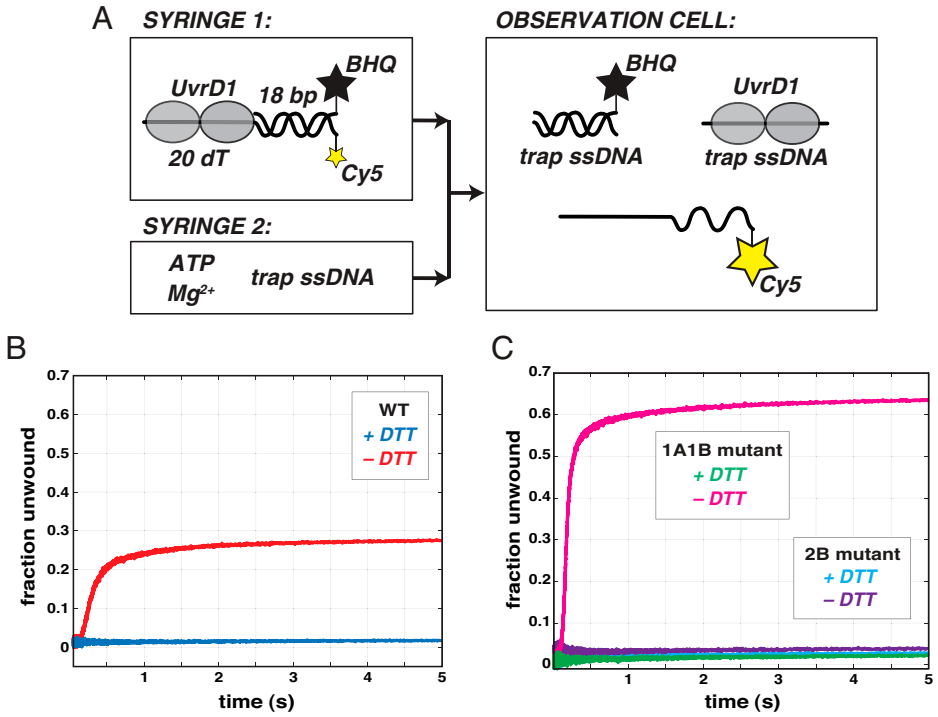

Fig. 4. Unwinding activity is dependent on redox-dependent dimer. (*A*) Stopped-flow assay for monitoring DNA unwinding. One syringe is filled with UvrD1 that has been preequilibrated with a fluorescently labeled unwinding template consisting of an 18-bp duplex with a 3′ single-stranded 20 dT tail. The 5′-end of the loading strand is labeled with Cy5, and the 3′-end of the other strand is labeled with BHQ. A second syringe is filled with ATP, Mg^{2+}, and single-stranded TRAP DNA. Upon mixing, UvrD1 unwinds some fraction of the DNA, resulting in a fluorescence enhancement due to the separation of the Cy5 from the BHQ. The excess TRAP DNA binds both the BHQ-labeled single strand and any free UvrD1 to establish single-round turnover conditions. (*B*) Fraction of DNA template unwound with 200 nM WT UvrD1 in the presence (blue) and absence (red) of DTT. (*C*) Fraction of DNA template unwound with 200 nM 1A1B double and 2B mutants of UvrD1 in the presence (green and cyan) and absence (pink and purple) of DTT in Buffer A with 75 mM NaCl.

and the BHQ2 strand is trapped via an excess of unlabeled complementary "TRAP" DNA, resulting in an increase in Cy5 fluorescence. This excess of TRAP also serves to bind any UvrD1 that dissociates from the labeled template, ensuring single-round turnover conditions (*SI Appendix*, Fig. S9*A*). UvrD1 was prebound to the labeled DNA template and was loaded in one syringe. This solution was rapidly mixed with the contents of the other syringe consisting of an excess of TRAP strand, 5 mM Mg^{+2}, and 1 mM ATP. The fraction of DNA unwound as a function of time was calculated by comparing experimental traces to a positive control consisting of fully single-stranded Cy5-labeled DNA and a negative control in the absence of ATP (*SI Appendix*, Fig. S9*B*).

In the absence of reducing agent, 200 nM WT UvrD1 can unwind ∼27% of 2 nM duplex DNA in a single-round reaction (Fig. 4*B*, red), consistent with the fraction dimer in these conditions (Fig. 1*A*). In addition, the kinetics and final percent unwound show a duplex length dependence, as is expected (*SI Appendix*, Fig. S10*A*). Fits to an n-step model with a nonproductive fraction (*SI Appendix*, Fig. S10 *A* and *B*) lead to an average unwinding rate of 64.8 ± 6.4 bp/s (*SI Appendix*, Table S2). Similarly, a lag time analysis (60, 61) yielded an estimate of the unwinding rate of 83.3 ± 12.3 bp/s (*SI Appendix*, Fig. S10 *C* and *D*). In contrast, in the presence of 1 mM DTT, which shifts the UvrD1 population to favor of monomers, no unwinding is observed, consistent with the UvrD1 dimer being required for unwinding activity (Fig. 4*B*, blue). In addition, the 2B mutant (C451A), which we have shown is an obligate monomer even under oxidative conditions, lacks helicase activity in both the presence and absence of DTT (Fig. 4*C*, cyan and purple). Consistently, the 1A1B double mutant is still able to unwind DNA in the absence of DTT (Fig. 4*C*, pink). In fact, the 1A1B double mutant unwinds a higher fraction of DNA than WT (∼63%), consistent with the area under the curve (analytical ultra-centrifugation [AUC]) results, suggesting that a higher fraction of the enzyme is in the dimeric form in the absence of DTT (Fig. 2*D*). Thus, the dimer fraction of UvrD1 formed via the 2B domain disulfide bond is required for DNA-unwinding activity under single-turnover conditions. Experiments under multiple-turnover conditions (i.e., in the absence of TRAP) recapitulated these results, as no unwinding was observed with monomeric UvrD1 (either WT + DTT or the 2B mutant) (*SI Appendix*, Fig. S11). This further suggests that even multiple monomer-binding events are not sufficient for unwinding activity.

Both Monomers and Dimers of UvrD1 Bind DNA. When considering why UvrD1 dimerization is required for DNA unwinding, we initially considered two hypotheses. The first hypothesis was that monomers are unable to bind DNA at the concentrations utilized, and the second hypothesis was that dimerization is required for helicase activation. To determine the nature of the DNA-bound species, we used sedimentation velocity to examine both WT UvrD1 and the 2B mutant in the absence of reducing agent and in the presence of fluorescently labeled 18-bp dT_{20} DNA. The results show that both monomers and dimers interact with the DNA and appear to bind the DNA in the same ratio as the free oligomeric forms. Specifically, in the presence of 1.5 μM WT UvrD1 and 1.5 μM DNA, 30% of the DNA was bound by monomers and 31% was bound by dimers (Fig. 5*A*, red, and *SI Appendix*, Table S3). In the presence of 1.5 μM of the 2B mutant, only monomers were bound to DNA (Fig. 5*A*, blue). Even at higher molar ratios of monomeric

Downloaded at SCHL MED LIB&77880003 on February 16, 2022

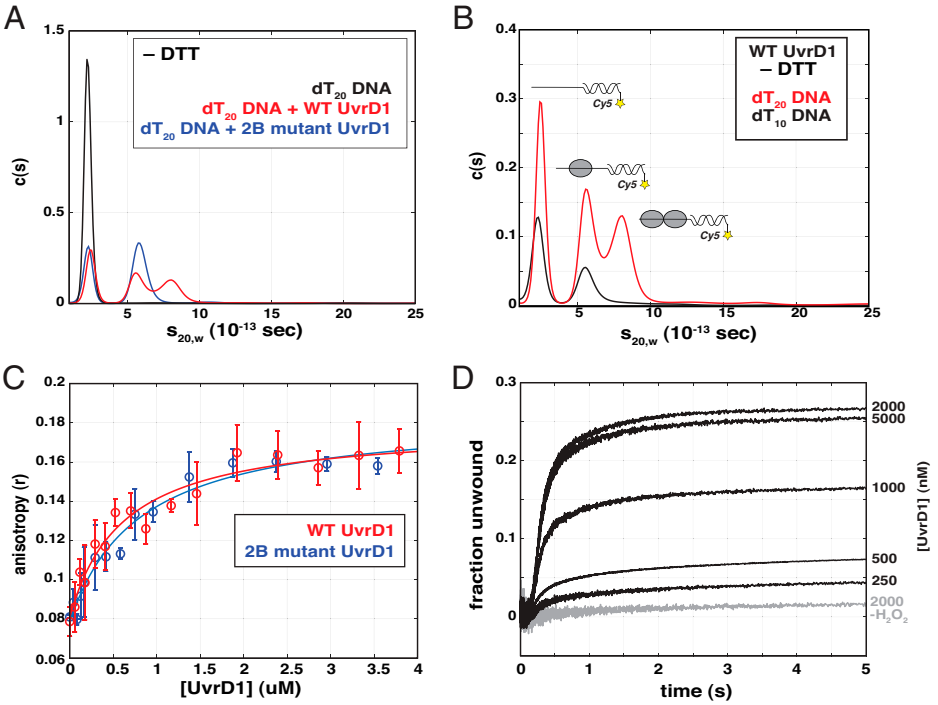

Fig. 5. Monomer and dimer forms of UvrD1 both bind DNA-unwinding template. (*A*) All experiments were performed in Buffer A with 75 mM NaCl. A Cy5-labeled DNA was used in sedimentation velocity experiments to specifically interrogate DNA-bound species. dT_{20} DNA alone (black), DNA and WT UvrD1 in the absence of reducing agent (red), and DNA and the 2B mutant in the absence of reducing agent (blue) are shown along with the bound species represented by each peak. (*B*) WT UvrD1 in the absence of reducing agent bound to dT_{20} and dT_{10} DNA templates. Both monomers and dimers bind dT_{20} (red), while only monomers bind dT_{10} (black). (*C*) Fluorescent anisotropy of a FAM-labeled helicase template DNA (dT_{20} ssDNA tail with 18-bp duplex) as a function of UvrD1 concentration. In the absence of DTT, both WT UvrD1 (red) and the 2B mutant (blue) displayed similar concentration dependencies of binding, suggesting that they bind this template with similar affinity. (*D*) DNA unwinding traces as a function of UvrD1 concentration first treated with 1 mM DTT, followed by the addition of 2 mM H_2O_2. A control in the absence of oxidizing agent is shown for comparison ($-H_2O_2$).

UvrD1 (i.e., the 2B mutant) to DNA, only monomers are observed bound to DNA, suggesting that DNA binding alone does not stimulate dimerization (*SI Appendix*, Fig. S12). In contrast, when WT UvrD1 in the absence of DTT is mixed with DNA possessing a shorter single-stranded extension (dT_{10}), only monomers bind (Fig. 5*B* and *SI Appendix*, Table S3), and no DNA unwinding is observed (*SI Appendix*, Fig. S13). This result is consistent with a model where each individual monomer interacts with the ssDNA in the context of the bound dimer, as is seen with *E. coli* UvrD (23). Fluorescent anisotropy experiments with the unwinding substrate DNA (18-bp dT_{20}) and either WT or 2B mutant UvrD1 yielded similar concentration dependencies of binding, consistent with the idea that the affinities of the monomeric and dimeric species are similar (Fig. 5*C*). Lastly, dissociation kinetics measured via a reduction in protein-stimulated fluorescence enhancement are also similar between WT and the 2B mutant (*SI Appendix*, Fig. S14) and indicate that there is no significant difference in residence time at the junction.

The observation of DNA-bound monomers with similar binding properties as the dimer directly eliminates the possibility that monomers do not unwind because they do not bind at the DNA junction and suggests that some other property of the dimer is required for unwinding. This is consistent with other studies of UvrD-family enzymes, as described in *Discussion*.

At a constant redox potential established by the addition of 2 mM H_2O_2, the expected protein concentration dependence of DNA unwinding is observed (Fig. 5*D*). Here, the fraction of DNA unwound saturates at ~27%, consistent with the fraction of dimers under these conditions (Fig. 1*D*), further suggesting that the monomers and dimers compete approximately equally for this DNA substrate under these conditions.

Both UvrD1 Monomers and Dimers Are ssDNA Translocases. As both monomers and dimers can bind to the DNA substrate (Fig. 5), we considered our second hypothesis that postulated that monomers are unable to translocate along ssDNA, thus preventing helicase activity. To test this, we examined the translocation kinetics of UvrD1 on ssDNA. Since UvrD1 has a 3′-to-5′ DNA-unwinding polarity, the kinetics of translocation were measured via stopped-flow assays (62, 63) by monitoring the arrival of UvrD1 at the 5′-end of a series of Cy3 5′-end–labeled oligodeoxythymidylate ssDNAs of different lengths (L = 20, 35, 45, 75, and 104 nucleotides) (Fig. 6*A*). Arrival of a translocating protein at the 5′-end results in an enhanced Cy3 fluorescence, and subsequent dissociation of UvrD1 leads to a return of the signal to baseline. A heparin concentration of 1 mg/mL was added to prevent rebinding of free UvrD1 to the ssDNA, ensuring single-round conditions (*SI Appendix*, Fig. S15*A*). In addition, negative controls in the absence of ATP showed no change in fluorescence (*SI Appendix*, Fig. S15*A*), and experiments containing ATP and UvrD1 in the presence of 3′-labeled DNA showed only a decay in fluorescence, consistent with translocation away from the dye (*SI Appendix*, Fig. S15*B*). In conditions favoring dimeric UvrD1, the presence of ATP resulted in the expected length-dependent peaks of fluorescence indicative of UvrD1 translocation in the 3′-to-5′ direction (62, 63) (*SI Appendix*, Fig. S16). However, monomeric UvrD1 generated either by the addition of DTT or the use of the 2B mutant also resulted in DNA length–dependent changes in the fluorescence signal, consistent with 3′-to-5′ ssDNA translocation (Fig. 6 *B* and *C*). Global analysis using an n-step sequential model (*SI Appendix*, Fig. S17) (62, 64) produced better fits for the 2B-mutant data, possibly because the WT UvrD1 still contains trace amounts

Downloaded at SCHL MED LIB&77680003 on February 16, 2022

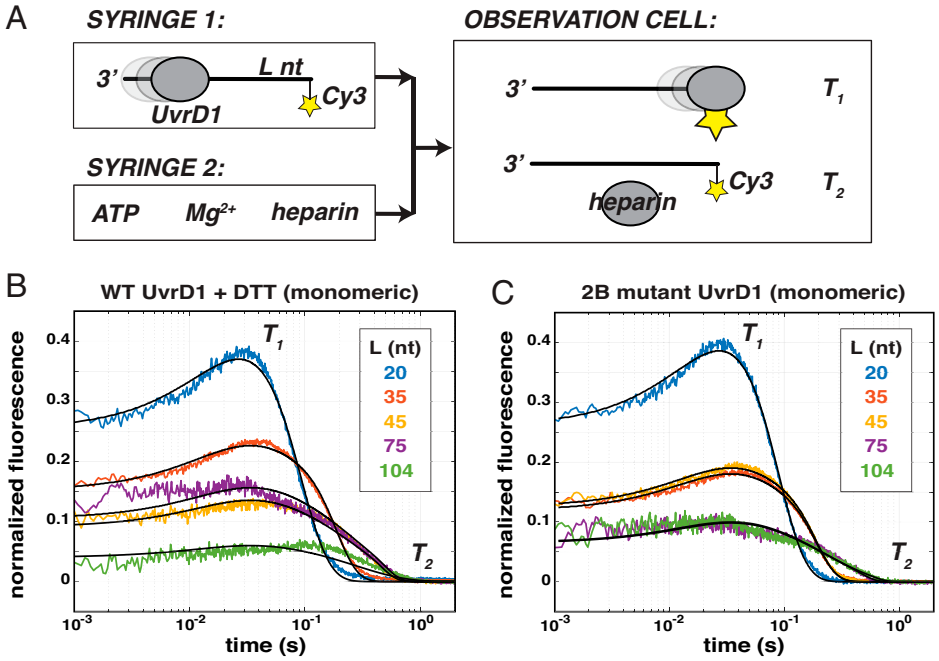

Fig. 6. Monomeric UvrD1 translocates on ssDNA. (*A*) The stopped-flow translocation assay. UvrD1 is allowed to equilibrate and bind to ssDNA templates of different lengths (*L*). These templates are labeled at the 5′-end with Cy3. The protein–DNA solution is mixed with buffer containing ATP, Mg^{2+}, and heparin to stimulate a single round of translocation. As the protein passes the label, the fluorescence increases (T_1). As it dissociates, the fluorescence decreases, and free protein is bound by heparin (T_2). (*B*) WT UvrD1 in the presence of 1 mM DTT produces traces consistent with translocation. The peak broadens and moves to longer times with increasing template lengths. (*C*) Monomeric UvrD1 generated by use of the 2B mutant also shows clear peaks, consistent with translocation. In both *B* and *C*, experiments were conducted in Buffer A with 75 mM NaCl, where the traces were normalized to the average of ten final plateau values observed in the raw data at each DNA length. Fits to an n-step sequential stepping model are shown in solid lines.

of dimer (*Materials and Methods* and *SI Appendix*, Fig. S18). However, fits of both data sets yielded consistent estimates of the macroscopic translocation rate (mk_t) of 120 ± 5 nucleotides/s (WT + DTT) and 130 ± 10 nucleotides/s (2B-DTT) for monomeric UvrD1, which is very similar to the ssDNA translocation rate measured for *E. coli* UvrD monomers (62, 63). In addition, the estimated dissociation rate (k_d) from the fitting analysis (4.1 ± 0.1 s^{-1}) was on the same order of magnitude as that obtained by experimental measures (8.1 ± 0.2 s^{-1}) (*SI Appendix*, Fig. S18). Other fit parameters are listed in *SI Appendix*, Table S4 (64).

The time courses exhibited under monomeric UvrD1 conditions were distinct from those collected under oxidative conditions, suggesting that the monomer and dimer populations exhibit distinct translocation kinetics (Fig. 6 *B* and *C* and *SI Appendix*, Fig. S16). Fits using the percent fraction of monomeric and dimeric species and the translocation parameters obtained under monomeric conditions resulted in estimates for the ssDNA translocation properties of the UvrD1 dimer (*SI Appendix*, Table S4). Although analysis of the mixed dimer/monomer population was challenging due to the presence of multiple species and kinetic phases, taken together, the data unequivocally show that both monomeric and dimeric UvrD1 translocate with 3′-to-5′ directionality along ssDNA.

DNA-Unwinding Activity Is Titrated by Redox Potential through Dimer Formation. We have shown that UvrD1 dimerization can be titrated via the addition of an oxidizing agent such as H_2O_2 (Fig. 1*D*). Furthermore, these dimers are, in the absence of other activators, required for DNA unwinding (Fig. 4). To determine the quantitative relationship between dimer fraction, DNA unwinding, and redox potential in millivolts (mV), we performed both sedimentation velocity and helicase assays using H_2O_2 to titrate redox potential. The 1A1B double mutant was used for these titrations to ensure that any effects stemmed directly from the cysteine in the 2B domain. We tested two different concentrations of the 1A1B double mutant (1 and 2 μM) in the presence of 1 mM DTT, which results in over 95% monomer (Fig. 2*D*) and shows no DNA unwinding (Fig. 4*C*). We then titrated H_2O_2 from 0 to 5 mM, which corresponds to redox potentials between −270 and 130 mV. As the redox potential became more positive (oxidizing), the fraction of DNA unwound increased (Fig. 7 and *SI Appendix*, Fig. S19, purple). As in the case of the WT UvrD1 (Fig. 1*D*), the fraction of UvrD1 1A1B double–mutant dimer also increased with increasing H_2O_2 (Fig. 7, orange). In fact, there is a quantitative correlation between the fraction of DNA unwound and the fraction of UvrD1-mutant dimer, consistent with the hypothesis that UvrD1 helicase activity is stimulated via increasing positive redox potentials found under oxidative conditions (Fig. 7 and *SI Appendix*, Fig. S19).

Discussion

Processive DNA helicases are enzymes that couple ATP binding and hydrolysis to translocation on ssDNA and unwinding of dsDNA and are involved in critical pathways throughout nucleic acid metabolism. The SF1 superfamily of helicases is the largest group of known helicases and includes UvrD, Rep, and PcrA (19, 20). These helicases consist of two RecA-like domains (1A and 2A) and two accessory subdomains (1B and 2B) (19, 20). Studies of SF1 helicases have shown that in the absence of accessory factors or force exerted on the DNA, individual monomers possess ssDNA translocase activity but not helicase activity; helicase activity requires at least a dimeric form of the enzyme (21, 22, 27, 28, 30, 32, 33, 62–64). Yet, the dimerization interface is not known, as crystal structures of UvrD and PcrA only reveal a monomer bound to DNA (65–68).

Previous studies of *Mtb* UvrD1 concluded that it is monomeric, as shown by size-exclusion chromatography (SEC) and

Downloaded at SCHL MED LIB&77880003 on February 16, 2022

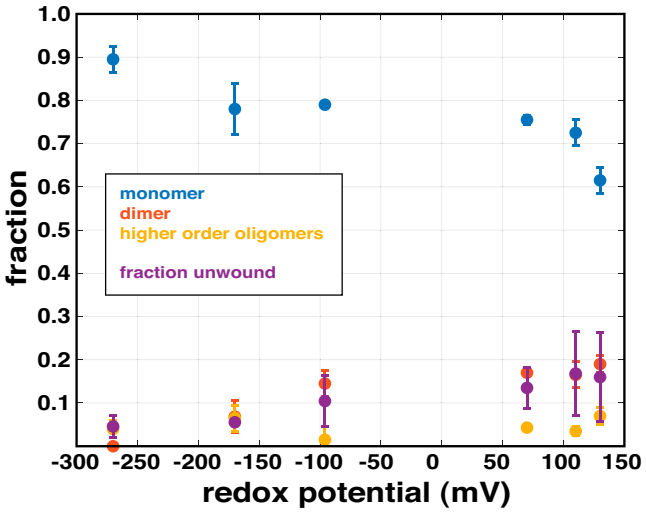

Fig. 7. Unwinding activity correlates with dimer fraction and is titrated by redox potential. The 1A1B double-mutant UvrD1 (1 μM) was dialyzed in Buffer A at 75 mM NaCl, treated with 1 mM DTT, and then incubated with varying concentrations of H_2O_2 (0 to 5 mM). Redox potential was measured, and the samples were subject to AUC and used for DNA-unwinding assays. The fraction of monomer present in different oligomeric states and fraction of DNA unwound are plotted as a function of redox potential as follows: monomer (blue), dimer (orange), higher-order oligomers (yellow), and fraction of DNA unwound (purple).

equilibrium sedimentation, and is capable of unwinding dsDNA in this form (45, 48). However, in one case, SEC and equilibrium sedimentation were performed in the presence of the reducing agent DTT, whereas DNA-unwinding assays were performed in its absence (48). In the other case, helicase activity of UvrD1 was attributed to monomers and was dependent on its binding partner Ku (45). When we purified *Mtb* UvrD1 without reducing agent, it eluted as two peaks on SEC, corresponding to the expected molecular weights of both monomer and dimer (*SI Appendix*, Fig. S1*A*). AUC experiments show that, while salt concentration had almost no effect on the amount of the dimeric form, the addition of DTT results in a dramatic shift to a single monomeric peak, suggesting that *Mtb* UvrD1 undergoes a cysteine-dependent dimerization (Fig. 1). We also observe a higher oligomeric species increasing in a concentration-dependent manner in sedimentation velocity experiments performed under oxidizing conditions. We do not observe higher-order oligomers of *Mtb* UvrD1 binding to the tailed construct used in our unwinding assays (Fig. 5*A*), but we cannot eliminate the possibility that this form could bind to DNA possessing longer single-stranded tails.

We identified a critical cysteine residue in the 2B domain of UvrD1 (C451) that is required for UvrD1 dimerization (Fig. 2). More specifically, the C451A mutation abrogated both dimerization and helicase activity, pointing to the existence of a 2B–2B disulfide–bonded dimer. The 2B domain of UvrD-like helicases has been described as an autoinhibitory domain (28, 32) that can adopt a range of rotational conformational states relative to the rest of the protein (30, 31, 34, 36, 69). The different 2B domain conformational states of the monomer are influenced by salt concentration, DNA binding, enzyme dimerization, and the binding of accessory protein factors (26, 34, 69, 70). For example, crystal structures of Rep bound to ssDNA showed Rep monomer bound to DNA in two different conformations (66). In one of the conformations, the 2B domain is in an "open" conformation, while in the other, the 2B domain is reoriented by a 130° swivel motion around a hinge region to contact the 1B domain. This swiveling motion closes the binding groove located between 1A, 1B, and 2A domains around the DNA template. Consistently, single-molecule and ensemble fluorescence resonance energy transfer studies have also shown that the 2B domain of a monomer can be in closed or open conformations (31, 34, 69–71). Furthermore, removing the 2B domain from Rep causes the Rep monomer to gain helicase activity (32). These observations and others have led to the hypothesis that the 2B domain is autoinhibitory for monomer helicase activity but serves as the interface between subunits within the functional Rep and UvrD dimers (19, 28, 30, 72). In this context, dimerization reorients the 2B domain to relieve its inhibitory properties, resulting in active dimers.

The formation of a 2B–2B disulfide bond in the case of *Mtb* UvrD1 fits well in this model, where 2B–2B-driven dimerization results in an active helicase conformation. Further support for this idea can be found in the specific location of C451. Mutations to 2B domain threonine residues, such as T426 of *B. stearothermophilus* PcrA and T422 of *E. coli* UvrD, disrupt helicase activity (73). This threonine residue is conserved in non-Actinobacteria UvrDs, is absent from UvrD-like proteins containing the cysteine residue described here, and is located two amino acids upstream to the C451 of *Mtb* UvrD1. The similar location of these residues suggests that UvrD-like helicases share a common 2B–2B dimerization interface and that mutating this threonine may destabilize the dimeric form of the enzyme. Interestingly, the 2B domains of the SF1 family members RecB and RecC interact in a RecBCD helicase complex (74). We aligned the UvrD1 2B domain sequence with the 2B domain sequences of *E. coli* RecB and RecC, which lack a 2B cysteine equivalent to C451. When we mapped residues that aligned close to the 2B cysteine onto the structure of RecBCD (PDB: 5LD2) (74, 75), we observed that these regions in RecB and RecC are only 10 to 15 Å apart. Again, this is consistent with our identification of the region surrounding the 2B cysteine of UvrD1 as an interface for 2B–2B domain–based activation of UvrD1-like helicases.

As noted, the 2B cysteine we have identified in *Mtb* UvrD1 appears unique to certain classes of Actinobacteria (Fig. 3). The 2B domain of *E. coli* UvrD does contain a cysteine residue at a different location (C441). However, experiments with *E. coli* UvrD showed no effect on oligomeric state with changes in redox potential (*SI Appendix*, Fig. S7).

Another pathway for stimulation of unwinding by UvrD family enzymes requires the binding of activating partners. The mismatch repair protein MutL can activate the monomer helicase activity of *E. coli* UvrD as well as stimulate the activity of UvrD dimers, and activation is accompanied by a change in the rotational state of the 2B domain (33). This interaction also leads to enhanced processivity, which enables UvrD to unwind longer stretches of DNA when functioning with MutL (32). Similarly, the accessory factor PriC can activate the Rep monomer helicase and stimulate the Rep dimer helicase (76). By analogy, the nonhomologous end joining factor *Mtb* Ku has been reported to bind to the C-terminal region of UvrD1 (45), suggesting a role for UvrD1 in double-strand break repair. As the results from our study show that UvrD1 can exist as a monomer or dimer depending on the redox potential, we are currently investigating whether Ku can activate the UvrD1 monomer helicase and/or stimulate dimer activity and whether it does this via modulation of the 2B domain conformation.

Mtb actually has two UvrD family members in its genome, UvrD1 and UvrD2, with UvrD1 being the homolog to *E. coli* UvrD (45–47, 77) and UvrD2 consisting of an N-terminal SF1 helicase motor linked to a helicase and RNase D C-terminal domain and tetracysteine motif domains (44, 78). The cysteines within the tetracysteine motif bind zinc, and the domain is required for helicase activity of UvrD2 in vitro (44). However, in this case, the activity appears to be dependent on the

Downloaded at SCHL MED LIB&77880003 on February 16, 2022

presence of the domain and not the presence of the individual cysteines themselves. Interestingly, while WT UvrD2 does not show a dependence on Ku, a truncated construct lacking the tetracysteine domain can be activated by Ku (44). Therefore, while both UvrD1 and UvrD2 utilize cysteine residues for helicase activity, they do so via distinct biochemical mechanisms.

During infection, *Mtb* resides within alveolar macrophages and neutrophils where it is exposed to reactive oxygen intermediates (ROI) and reactive nitrogen intermediates (RNI) that cause DNA damage (49, 79, 80). *Mtb* lacks mismatch repair (81), and the response of *Mtb* to these insults likely involves NER pathways (79). During NER, UvrD1 unwinds the damaged DNA strand to remove bulky lesions that have been recognized by UvrA/UvrB and excised by UvrC (2). Analysis of gene expression data has shown UvrA to be highly expressed during oxidative stress (82). In addition, both *uvrD1/uvrB* and *uvrD1/uvrA* double mutants in *M. smegmatis* have been shown to be more sensitive to tertiary butyl hydroperoxide and acidified nitrite than WT strains (46, 83). All of these observations suggest a role of NER enzymes, including UvrD1, during oxidative stress in *Mtb*. This is distinct from *E. coli*, in which repair of RNI- and ROI-induced DNA damage is accomplished by base excision repair and homologous recombination (84). Thus, the redox-dependent dimerization of UvrD1 we report here may represent an important mechanism in *Mtb* underlying the repair of oxidative-dependent DNA damage during infection.

Materials and Methods

Cloning, Overexpression, and Purification of *Mtb* UvrD1. *Mtb* UvrD1 (Rv0949) from H37Rv was cloned in the expression vector pET with a SUMO-His tag at the N terminus and kanamycin resistance. It was PCR amplified with BamH1 at the 5′-end and HindIII at the 3′-end. The UvrD1 2B domain cysteine-to-alanine substitution and 1A1B double cysteine-to-threonine substitution mutations were introduced into the *Mtb* UvrD1 plasmid by PCR amplification using primers and a site-directed mutagenesis kit (Agilent, 200521). Sequences for all primers and a list of plasmids can be found in *SI Appendix*, Table S5. The inserts of all UvrD1 plasmids were sequenced to exclude the acquisition of unwanted coding changes during amplification or cloning. The pET-*Mtb* UvrD1 plasmids were transformed into *E. coli* BL21(DE3). Cultures (3 L) were grown at 37 °C in a Luria-Bertani medium containing 50 mg/mL kanamycin until the absorbance at 600 nm (A_{600}) reached ∼0.5. The cultures were chilled on ice for about 1 h, and the expression of recombinant protein was induced around 0.55 optical density (OD) with 0.25 mM isopropyl-β-D-thiogalactopyranoside, followed by incubation at 16 °C for 16 h with constant shaking. The cells were harvested by centrifugation, and the pellets were either stored at −80 °C or used for subsequent procedures that were performed at 4 °C. The bacterial cells from the 3-L culture were resuspended in 50 to 75 mL of lysis buffer (50 mM Tris-HCl, pH 7.5, 0.25 M NaCl, and 10% sucrose). Lysozyme and Triton X-100 were added to final concentrations of 1 mg/mL and 0.1%, respectively. At the time of lysis, a complete ethylenediaminetetraacetic acid (EDTA)-free protease inhibitor mixture (Sigma, 118735800) was added to the lysate. Next the lysates were sonicated, and insoluble material was removed by centrifugation at 23,400 g for 45 min. The soluble extracts were applied to 2-mL columns of nickel-nitrilotriacetic acid agarose (Ni-NTA) (QIAGEN, 30210) that had been equilibrated with lysis buffer without protease inhibitors. The columns were washed with 10× column volume of wash buffer (50 mM Tris-HCl, pH 8.0, 0.25 M NaCl, 0.05% Triton X-100, and 10% glycerol) and then eluted stepwise with wash buffer containing 50, 100, 200, 500, and 1,000 mM imidazole. The polypeptide compositions of the column fractions were monitored by sodium dodecyl sulphate-polyacrylamide gel electrophoresis (SDS-PAGE). The His-SUMO–tagged UvrD1 polypeptides were recovered predominantly in the 100- and 200-mM imidazole eluates. Fractions containing the UvrD1 protein were pooled, and His-tagged Ulp1 protease was added (at a ratio of 1:500 [wt/wt] protease per protein) and dialyzed against dialysis buffer (50 mM Tris-HCl, pH 8.0, 1 mM EDTA, 0.1% Triton X-100, and 10% glycerol) containing 150 mM NaCl overnight. The SUMO-cut UvrD1 was then incubated with Ni-NTA agarose for about 3 h, and the untagged UvrD1 (cleaved) was recovered in the flow-through and wash fractions. After pooling and concentrating the fractions by VIVASPIN centrifugal filters (30-kDa cutoff, Sartorius, VS2021), the protein was loaded on a heparin HiTRAP column (Cytiva, 17040701) (5 mL × 2) preequilibrated with dialysis buffer containing 150 mM NaCl. Upon running a linear gradient from 200 to 800 mM NaCl, the protein eluted at ∼400 mM NaCl. The fractions with a single band on a reducing SDS-PAGE corresponding to the molecular weight of a monomer were pooled together and concentrated to load on the S300 sizing column (HiPrep 16/60 Sephacryl S-300 HR column, Cytvia, 17116701) in buffer (150 mM NaCl, 10% glycerol, and Tris, pH 8.0) at 25 °C without DTT. The peak fractions were pooled and stored at −80 °C at concentrations of about 15 to 20 μM. Both the 2B mutant and 1A1B double mutant were overexpressed and purified in a manner similar to the WT UvrD1 protein.

Homology Modeling of *Mtb* UvrD1. The predicted structure of *Mtb* UvrD1 was obtained using PHYRE2 (85) by submitting the amino acid sequence of *Mtb* UvrD1. The PDB reference used for modeling the open structure of *Mtb* UvrD1 was *E. coli* UvrD 3LFU and for modeling the closed structure was *B. stearothermophilus* PcrA helicase complex 3PJR. Solvent accesible surface area (SASA) calculations were done in Chimera (53).

Phylogeny Analysis of *Mtb* UvrD1. The protein sequence of *Mtb* UvrD1 obtained from UniProt (https://www.uniprot.org/uniprot/P9WMQ1.fasta) was used to BLAST against various genus and species of classes of the phylum Actinobacteria (https://blast.ncbi.nlm.nih.gov/Blast.cgi). Two to three genera of orders in which the cysteine in the 2B domain is conserved were chosen and aligned in Clustal omega (86), and the phylogenetic tree was plotted using NJ plot (87).

Analytical SEC. One milliliter of *Mtb* UvrD1 (30 μM) was injected in an S300 gel filtration column at a flow rate of 0.25 mL/min, monitoring absorbance at 280 nm for a measure of the elution volume (V) in buffer (150 mM NaCl, 10% glycerol, and Tris, pH 8.0). The value of V_e/V_o (elution volume/void volume) was interpolated using the generated standard curve (Bio-Rad gel filtration standard, 1511901) to yield the estimated molecular weight of *Mtb* UvrD1 monomer (90-kDa) and dimer (170-kDa) fractions.

DNA Substrates. ssDNA, which was labeled with Cy5, Cy3, fluorescein (FAM), or BHQ2, was ordered from IDT. For annealing of the oligos, the Cy5 label at the 5′-end of the ssDNA was mixed with an equimolar concentration of unlabeled complementary strand or complementary strand labeled with BHQ2 in 10 mM Tris, pH 8.0, and 50 mM NaCl, followed by heating to 95 °C for 5 min and slow cooling to room temperature.

Synthesis of Poly-dT. The homodeoxypolynucleotide poly-dT substrate was used to measure the dissociation rate from internal sites of ssDNA. Since the poly-dT from commercial sources is polydisperse, we prepared samples using enzyme-terminal deoxynucleotidyl transferase (TdTase) from calf thymus glands to catalyze polymerization of deoxynucleotide triphosphate into poly-dT of more well-defined lengths (88). The protocol includes mixing dT_{100} with potassium cacodylate buffer, potassium chloride, cobalt chloride, inorganic pyrophosphatase (Thermo Fisher Scientific, EF0221), deoxythymidine-5′-triphosphate (Thermo Fisher Scientific, R0171), and TdTase (Thermo Fisher Scientific, 10533065). The reaction was kept at room temperature for 3 to 4 d, and poly-dT was purified using phenol–chloroform extraction and suspending the air-dried pellet in water. The weight average length of the poly-dT was determined by measuring the weight average sedimentation coefficient by boundary sedimentation velocity experiments using AUC. The weight average length determined from this method is 964 nucleotides and was determined using a method from the measured weight average sedimentation coefficient on poly-U (89).

Analytical Ultracentrifugation. The analytical ultracentrifugation sedimentation velocity experiments were performed using a Proteome Lab XL-A analytical ultracentrifuge equipped with an An50Ti rotor (Beckman Coulter). The sample (380 μL) and buffer (410 μL) were loaded into each sector of an Epon charcoal-filled two-sector centerpiece. All experiments were performed at 25 °C and 42,000 rpm. Absorbance data were collected by scanning the sample cells at intervals of 0.003 cm, monitoring either at 230 nm, 280 nm or 650 nm depending on protein/DNA concentration, to maintain an absorbance signal between 0.1 and 1. Both the DNA and protein samples were dialyzed in buffer (75 mM NaCl, 20% glycerol, and 10 mM Tris, pH 8.0) except the salt titration where the protein was dialyzed in different salts in 20% glycerol and 10 mM Tris, pH 8.0.

Continuous sedimentation coefficient distributions, $c(s)$, were calculated using SEDFIT(6, 92), truncating the fit at 7.0 radial position to avoid contributions of glycerol buildup (90). This analysis yielded individual sedimentation coefficients for each monomer, dimer, and higher-order species as well as a weighted average frictional coefficient (f/f_o) for the entire distribution (*SI Appendix*, Table S1). Calculated sedimentation coefficients were converted to 20 °C water conditions ($s_{20,w}$) according to

$$s_{20,w} = s_{exp}\frac{\eta_{exp}}{\eta_{20,w}}\left(\frac{1-\bar{\upsilon}_{20}\,\rho_{20,w}}{1-\bar{\upsilon}_{exp}\,\rho_{exp}}\right),$$

BIOCHEMISTRY

Downloaded at SCHL MED LIB&77680003 on February 16, 2022

where $\rho_{20,w}$ and $\eta_{20,w}$ are the density and viscosity of water at 20 °C, ρ_{exp} and η_{exp} are the density and viscosity of the buffer at the experimental temperature of 25 °C, and $\bar{\upsilon}_{20}$ and $\bar{\upsilon}_{exp}$ are partial specific volumes of the protein at 20 °C and at 25 °C. Buffer densities, (ρ_{exp}) and viscosities (η_{exp}) were calculated from buffer composition using SEDNTERP (91). Partial specific volumes ($\bar{\upsilon}_{exp}$) for *Mtb* UvrD1 and point mutations were calculated in SEDNTERP using the amino acid composition. Integration of the entire *c*(*s*) distribution versus the integration of an individual sedimentation species was performed and used to calculate the population fraction (92).

For AUC experiments done in the presence of Cy5-labeled DNA, the absorbance signal was collected by scanning the sample cells at 650 nm. Partial specific volumes ($\bar{\upsilon}_{exp}$) for labeled DNA and the UvrD1–DNA complex were calculated according to

$$\bar{\upsilon} = \frac{(\sum_{i=1}^{n} n_i M_i \bar{\upsilon}_i)}{\sum_{i=1}^{n} n_i M_i}.$$

For AUC experiments conducted at different redox potentials, the protein was first dialyzed in Buffer A with 75 mM NaCl, and then 1 mM DTT was added at a respective concentration and titrated with a range of H_2O_2 from 0.5 to 2 mM. Redox potential was measured via a Metler Toledo Redox microelectrode (UX-35902-33). After H_2O_2 treatment, protein was incubated at room temperature for 2 h before performing AUC.

Stopped-Flow dsDNA-Unwinding Assay. All stopped-flow experiments were carried out at 25 °C using an Applied Photophysics instrument SX-20, total shot volume of 100 μL, and dead time of 1 ms. All experiments were carried out in buffer with Tris, pH 8.0, 75 mM NaCl, and 20% glycerol in the absence or presence of 1 mM DTT. Cy5 fluorophore was excited using a 625-nm light-emitting diode (LED; Applied Photophysics Ltd.), and its fluorescence emission was monitored at wavelengths >665 nm using a long-pass filter (Newport Optics). The traces represent the average of five independent shots and at least two different protein purifications. In this assay, a double-stranded 18-bp DNA with a T_{20}/T_{10} tail with Cy5 fluorophore is attached to the long strand, and BHQ_2 is attached to the short strand (*SI Appendix*, Table S6). The concentrations mentioned are the final concentrations after mixing the contents of both syringes. UvrD1 (200 nM) was incubated with 2 nM DNA in one syringe, which was then rapidly mixed with the contents of another syringe that consisted of TRAP, a complementary DNA strand in excess protein (25×, 5 μM), Mg^{+2} (5 mM), and ATP (1 mM). The concentrations of ATP and Mg^{+2} used were determined to be optimal for the *Mtb* UvrD1 unwinding assays (48). DNA strand separation is accompanied by an increase in the fluorescence signal. The unwinding signal was normalized to the signal from positive and negative controls to get the fraction of DNA unwound. The positive control was 2 nM dsDNA with BHQ2 on the short strand and Cy5 on the long strand that is denatured in the presence of TRAP, and 200 nM UvrD1 was added at room temperature to get maximum fluorescence signal. The negative control was the average fluorescence value recorded for the fully annealed DNA (2 nM) with UvrD1 (200 nM) shot against buffer alone. To get DNA unwinding with a change in redox potential, the protein was dialyzed, treated with DTT, and titrated with H_2O_2 in a similar way as was done for AUC experiments and incubated with DNA. This protein–DNA mix was then used for unwinding experiments.

Stopped-Flow ssDNA Translocation Assays. The kinetics of UvrD1 monomer and dimer translocation was examined in a stopped-flow experiment by monitoring the arrival of UvrD1 of a series of oligodeoxythymidylate lengths (L = 20, 35, 45, 64, 75, 94, and 104 nucleotides) labeled at the 5′-end with Cy3 (*SI Appendix*, Table S6) (62). Cy3 fluorescence was excited using a 535-nm LED with a 550-nm short-pass cutoff filter, and emission was monitored at >570 nm using a long-pass filter (Newport Optics). UvrD1 was preincubated with ssDNA in one syringe, and reactions were initiated by 1:1 mixing with 1 mM ATP, 5 mM $MgCl_2$, and heparin at a concentration of 1 mg/mL to prevent rebinding of UvrD1 (50 nM) to DNA (100 nM). Excess DNA-to-UvrD1 ratio was used to prevent binding of more than one UvrD1 monomer on DNA (62). Global analysis of time courses using the n-step sequential model was done to calculate various translocation parameters. For making heparin solution to be used as a TRAP for protein, ensuring single-round conditions, heparin sodium salt (porcine intestinal mucosa, Millipore Sigma, H3393) was dialyzed into Buffer A plus 75 mM NaCl, and concentrations were determined by an Azure A standard curve (93).

Tryptophan Fluorescence-Based Dissociation Kinetics. Dissociation kinetics of UvrD1 were monitored by the increase in UvrD1 tryptophan fluorescence excited using a 290-nm LED (Applied Photophysics Ltd.), and emission was monitored at >305 nm using a long-pass filter. The observed dissociation rate from internal ssDNA sites for UvrD1 monomer (with 1 mM DTT) and dimer (no DTT) was measured using dT_{100} and poly-dT oligos (average length of 964 nucleotides; *Synthesis of Poly-dT*), respectively. In one syringe, UvrD1 (100 nM) was added with DNA (50 nM) (concentrations listed are after equal volume mixing). In another syringe, ATP, $MgCl_2$, and heparin were added at the same concentrations as translocation assays, and the observed dissociation kinetic traces were best fit to a single exponential using ProData Viewer (Applied Photophysics). All experiments were performed at 25 °C in Buffer A with 75 mM NaCl and represent the average of five independent shots (88) For measuring dissociation kinetics from the single-stranded/double-stranded junction, 50 nM 18-bp DNA with a dT_{20} tail and a Cy3 fluorophore at the 3′-end of the long strand was preincubated with 400 nM UvrD1 (final concentrations after mixing) and shot against buffer with TRAP (5 μM) without ATP. The dissociation of UvrD1 from the DNA was monitored over time and fit using a single exponential function. All experiments were performed at 25 °C in Buffer A with 75 mM NaCl, and the data presented are from an average of five independent shots.

ssDNA Translocation and Unwinding Fitting Analysis. The translocation and the unwinding data were fit using the code from https://github.com/ordabayev/global-fit, and unwinding and translocation rates were calculated. Globalfit is a wrapper around lmfit (https://lmfit.github.io/lmfit-py/), providing an interface for multiple curves fitting with global parameters. Python 3 was installed via Anaconda along with modules such as numpy, scipy, matpotlib, lmfit, emcee, corner, os, and pandas, and then the globalfit model was used to fit the data for unwinding using the n-step unwinding model and translocation using a two-step dissociation model (64).

Steady-State Anisotropy Measurements. All fluorescence titrations were performed using a spectrofluorometer (ISS) equipped with Glan–Thompson polarizers. Measurements of the anisotropy and total fluorescence intensity of FAM-labeled dsDNA 18 bp with a dT_{20} single-stranded tail were recorded using excitation and emission wavelengths of 490 and 522 nm, respectively, using

$$r = \frac{I_{VV} - GI_{VH}}{I_{VV} + 2GI_{VH}},$$

where $I_{TOT} = I_{VV} + 2GI_{VH}$, where r is anisotropy, I_{TOT} is total intensity, I_{VV} and I_{VH} are fluorescence intensity of vertically and horizontally polarized emission and G is the G factor (94). The recorded value of G factor remained between 0.85 and 0.9 throughout the titrations. Titrations were performed using a Starna cells cuvette (16.100F-Q-10/Z15) with dimensions 12.5 × 12.5 × 45 mm and a pathlength of 1 cm. The protein was mixed three to four times with DNA during titrations and allowed to sit for 5 min before recording anisotropy values. The total volume of added protein was 30% of the initial volume, and as a control, dilution with buffer with the same volume of DNA alone did not change the anisotropy value. All titrations were conducted in Buffer A at 25 °C in 75 mM NaCl. The data represent the average from three independent experiments for WT-DTT and two independent experiments for the 2B mutant.

Data Availability. All study data are included in the article and/or *SI Appendix*.

ACKNOWLEDGMENTS. This work was supported by NIH R01 GM134362 to E.A.G., NIH R35 GM136632 to T.M.L., and by NIH T32 AI007172 to A.C. The content is solely the responsibility of the authors and does not necessarily represent the official views of the National Institutes of Health.

1. A. Sancar, DNA excision repair. *Annu. Rev. Biochem.* **65**, 43–81 (1996).
2. Y. Peng, H. Wang, L. Santana-Santos, C. Kisker, B. van Houten, "Nucleotide excision repair from bacteria to humans: Structure–function studies" in *Chemical Carcinogenesis*, T. M. Penning, Ed. (Springer, Cham, Switzerland, 2011), pp. 267–296.
3. C. Kisker, J. Kuper, B. Van Houten, Prokaryotic nucleotide excision repair. *Cold Spring Harb. Perspect. Biol.* **5**, a012591 (2013).
4. K. Howan *et al.*, Initiation of transcription-coupled repair characterized at single-molecule resolution. *Nature* **490**, 431–434 (2012).
5. A. J. Smith, N. J. Savery, RNA polymerase mutants defective in the initiation of transcription-coupled DNA repair. *Nucleic Acids Res.* **33**, 755–764 (2005).
6. B. Pani, E. Nudler, Mechanistic insights into transcription coupled DNA repair. *DNA Repair (Amst.)* **56**, 42–50 (2017).
7. V. Kamarthapu, E. Nudler, Rethinking transcription coupled DNA repair. *Curr. Opin. Microbiol.* **24**, 15–20 (2015).
8. G. Kokic *et al.*, Structural basis of TFIIH activation for nucleotide excision repair. *Nat. Commun.* **10**, 2885 (2019).
9. V. Oksenych, B. Bernardes de Jesus, A. Zhovmer, J. M. Egly, F. Coin, Molecular insights into the recruitment of TFIIH to sites of DNA damage. *EMBO J.* **28**, 2971–2980 (2009).
10. E. Compe, J. M. Egly, TFIIH: When transcription met DNA repair. *Nat. Rev. Mol. Cell Biol.* **13**, 343–354 (2012).

Downloaded at SCHL MED LIB&77680003 on February 16, 2022

11. R. R. Iyer, A. Pluciennik, V. Burdett, P. L. Modrich, DNA mismatch repair: Functions and mechanisms. *Chem. Rev.* **106**, 302–323 (2006).
12. C. Bruand, S. D. Ehrlich, UvrD-dependent replication of rolling-circle plasmids in *Escherichia coli*. *Mol. Microbiol.* **35**, 204–210 (2000).
13. G. F. Moolenaar, C. Moorman, N. Goosen, Role of the *Escherichia coli* nucleotide excision repair proteins in DNA replication. *J. Bacteriol.* **182**, 5706–5714 (2000).
14. M. J. Florés, N. Sanchez, B. Michel, A fork-clearing role for UvrD. *Mol. Microbiol.* **57**, 1664–1675 (2005).
15. R. C. Heller, K. J. Marians, Non-replicative helicases at the replication fork. *DNA Repair (Amst.)* **6**, 945–952 (2007).
16. H. M. Arthur, R. G. Lloyd, Hyper-recombination in uvrD mutants of *Escherichia coli* K-12. *Mol. Gen. Genet.* **180**, 185–191 (1980).
17. X. Veaute *et al.*, UvrD helicase, unlike Rep helicase, dismantles RecA nucleoprotein filaments in *Escherichia coli*. *EMBO J.* **24**, 180–189 (2005).
18. V. Petrova *et al.*, Active displacement of RecA filaments by UvrD translocase activity. *Nucleic Acids Res.* **43**, 4133–4149 (2015).
19. T. M. Lohman, E. J. Tomko, C. G. Wu, Non-hexameric DNA helicases and translocases: Mechanisms and regulation. *Nat. Rev. Mol. Cell Biol.* **9**, 391–401 (2008).
20. K. D. Raney, A. K. Byrd, S. Aarattuthodiyil, Structure and mechanisms of SF1 DNA helicases. *Adv. Exp. Med. Biol.* **767**, 17–46 (2013).
21. M. S. Dillingham, D. B. Wigley, M. R. Webb, Demonstration of unidirectional single-stranded DNA translocation by PcrA helicase: Measurement of step size and translocation speed. *Biochemistry* **39**, 205–212 (2000).
22. M. S. Dillingham, D. B. Wigley, M. R. Webb, Direct measurement of single-stranded DNA translocation by PcrA helicase using the fluorescent base analogue 2-aminopurine. *Biochemistry* **41**, 643–651 (2002).
23. N. K. Maluf, C. J. Fischer, T. M. Lohman, A dimer of *Escherichia coli* UvrD is the active form of the helicase in vitro. *J. Mol. Biol.* **325**, 913–935 (2003).
24. E. J. Tomko, C. J. Fischer, A. Niedziela-Majka, T. M. Lohman, A nonuniform stepping mechanism for *E. coli* UvrD monomer translocation along single-stranded DNA. *Mol. Cell* **26**, 335–347 (2007).
25. A. Niedziela-Majka, M. A. Chesnik, E. J. Tomko, T. M. Lohman, *Bacillus stearothermophilus* PcrA monomer is a single-stranded DNA translocase but not a processive helicase in vitro. *J. Biol. Chem.* **282**, 27076–27085 (2007).
26. N. K. Maluf, T. M. Lohman, Self-association equilibria of *Escherichia coli* UvrD helicase studied by analytical ultracentrifugation. *J. Mol. Biol.* **325**, 889–912 (2003).
27. K. S. Lee, H. Balci, H. Jia, T. M. Lohman, T. Ha, Direct imaging of single UvrD helicase dynamics on long single-stranded DNA. *Nat. Commun.* **4**, 1878 (2013).
28. K. M. Brendza *et al.*, Autoinhibition of *Escherichia coli* Rep monomer helicase activity by its 2B subdomain. *Proc. Natl. Acad. Sci. U.S.A.* **102**, 10076–10081 (2005).
29. S. Arslan, R. Khafizov, C. D. Thomas, Y. R. Chemla, T. Ha, Protein structure. Engineering of a superhelicase through conformational control. *Science* **348**, 344–347 (2015).
30. B. Nguyen, Y. Ordabayev, J. E. Sokoloski, E. Weiland, T. M. Lohman, Large domain movements upon UvrD dimerization and helicase activation. *Proc. Natl. Acad. Sci. U.S.A.* **114**, 12178–12183 (2017).
31. M. J. Comstock *et al.*, Protein structure. Direct observation of structure-function relationship in a nucleic acid-processing enzyme. *Science* **348**, 352–354 (2015).
32. M. A. Makurath, K. D. Whitley, B. Nguyen, T. M. Lohman, Y. R. Chemla, Regulation of Rep helicase unwinding by an auto-inhibitory subdomain. *Nucleic Acids Res.* **47**, 2523–2532 (2019).
33. Y. A. Ordabayev, B. Nguyen, A. Niedziela-Majka, T. M. Lohman, Regulation of UvrD helicase activity by MutL. *J. Mol. Biol.* **430**, 4260–4274 (2018).
34. Y. A. Ordabayev, B. Nguyen, A. G. Kozlov, H. Jia, T. M. Lohman, UvrD helicase activation by MutL involves rotation of its 2B subdomain. *Proc. Natl. Acad. Sci. U.S.A.* **116**, 16320–16325 (2019).
35. E. J. Gwynn *et al.*, The conserved C-terminus of the PcrA/UvrD helicase interacts directly with RNA polymerase. *PLoS One* **8**, e78141 (2013).
36. K. Sanders *et al.*, The structure and function of an RNA polymerase interaction domain in the PcrA/UvrD helicase. *Nucleic Acids Res.* **45**, 3875–3887 (2017).
37. V. Epshtein *et al.*, UvrD facilitates DNA repair by pulling RNA polymerase backwards. *Nature* **505**, 372–377 (2014).
38. World Health Organization, "Global tuberculosis report 2020" (2020). https://www.who.int/publications/i/item/9789240013131. Accessed 10 February 2022.
39. D. Jensen, A. R. Manzano, J. Rammohan, C. L. Stallings, E. A. Galburt, CarD and RbpA modify the kinetics of initial transcription and slow promoter escape of the *Mycobacterium tuberculosis* RNA polymerase. *Nucleic Acids Res.* **47**, 6685–6698 (2019).
40. H. Boyaci, R. M. Saecker, E. A. Campbell, Transcription initiation in mycobacteria: A biophysical perspective. *Biochem. Soc. Symp.* **11**, 53–65 (2019).
41. C. Bertrand, A. Thibessard, C. Bruand, F. Lecointe, P. Leblond, Bacterial NHEJ: A never ending story. *Mol. Microbiol.* **111**, 1139–1151 (2019).
42. J. Chen, H. Boyaci, E. A. Campbell, Diverse and unified mechanisms of transcription initiation in bacteria. *Nat. Rev. Microbiol.* **19**, 95–109 (2021).
43. R. Hershberg *et al.*, High functional diversity in *Mycobacterium tuberculosis* driven by genetic drift and human demography. *PLoS Biol.* **6**, e311 (2008).
44. K. M. Sinha, N. C. Stephanou, M.-C. Unciuleac, M. S. Glickman, S. Shuman, Domain requirements for DNA unwinding by mycobacterial UvrD2, an essential DNA helicase. *Biochemistry* **47**, 9355–9364 (2008).
45. K. M. Sinha, N. C. Stephanou, F. Gao, M. S. Glickman, S. Shuman, Mycobacterial UvrD1 is a Ku-dependent DNA helicase that plays a role in multiple DNA repair events, including double-strand break repair. *J. Biol. Chem.* **282**, 15114–15125 (2007).
46. K. M. Sinha, M. S. Glickman, S. Shuman, Mutational analysis of *Mycobacterium* UvrD1 identifies functional groups required for ATP hydrolysis, DNA unwinding, and chemomechanical coupling. *Biochemistry* **48**, 4019–4030 (2009).
47. J. Houghton *et al.*, Important role for *Mycobacterium tuberculosis* UvrD1 in pathogenesis and persistence apart from its function in nucleotide excision repair. *J. Bacteriol.* **194**, 2916–2923 (2012).
48. E. Curti, S. J. Smerdon, E. O. Davis, Characterization of the helicase activity and substrate specificity of *Mycobacterium tuberculosis* UvrD. *J. Bacteriol.* **189**, 1542–1555 (2007).
49. H. T. Pacl, V. P. Reddy, V. Saini, K. C. Chinta, A. J. C. Steyn, Host-pathogen redox dynamics modulate *Mycobacterium tuberculosis* pathogenesis. *Pathog. Dis.* **76**, fty036 (2018).
50. M. Mehta, A. Singh, *Mycobacterium tuberculosis* WhiB3 maintains redox homeostasis and survival in response to reactive oxygen and nitrogen species. *Free Radic. Biol. Med.* **131**, 50–58 (2019).
51. S. Upadhyay, E. Mittal, J. A. Philips, Tuberculosis and the art of macrophage manipulation. *Pathog. Dis.* **76**, fty037 (2018).
52. P. Schuck, Size-distribution analysis of macromolecules by sedimentation velocity ultracentrifugation and Lamm equation modeling. *Biophys. J.* **78**, 1606–1619 (2000).
53. E. F. Pettersen *et al.*, UCSF Chimera—A visualization system for exploratory research and analysis. *J. Comput. Chem.* **25**, 1605–1612 (2004).
54. H. Sowani, M. Kulkarni, S. Zinjarde, V. Javdekar, "*Gordonia* and related genera as opportunistic human pathogens causing infections of skin, soft tissues, and bones" in *The Microbiology of Skin, Soft Tissue, Bone and Joint Infections*, K. Kon, M. Rai, Eds. (Academic Press, Cambridge, MA, 2017), pp. 105–121.
55. M. Goodfellow, A. L. Jones, Bergey's Manual of Systematics of Archaea and Bacteria. 1–14 (John Wiley & Sons, Inc., 2020).
56. A. Gupta, A. N. Ananthakrishnan, Economic burden and cost-effectiveness of therapies for *Clostridiodes difficile* infection: A narrative review. *Therap. Adv. Gastroenterol.* **14**, 17562848211018654 (2021).
57. P.-J. Chiu *et al.*, *Clostridioides difficile* spores stimulate inflammatory cytokine responses and induce cytotoxicity in macrophages. *Anaerobe* **70**, 102381 (2021).
58. W. Cheng, J. Hsieh, K. M. Brendza, T. M. Lohman, *E. coli* Rep oligomers are required to initiate DNA unwinding in vitro. *J. Mol. Biol.* **310**, 327–350 (2001).
59. S. A. E. Marras, F. R. Kramer, S. Tyagi, Efficiencies of fluorescence resonance energy transfer and contact-mediated quenching in oligonucleotide probes. *Nucleic Acids Res.* **30**, e122 (2002).
60. J. A. Ali, T. M. Lohman, Kinetic measurement of the step size of DNA unwinding by *Escherichia coli* UvrD helicase. *Science* **275**, 377–380 (1997).
61. C. G. Wu, C. Bradford, T. M. Lohman, *Escherichia coli* RecBC helicase has two translocase activities controlled by a single ATPase motor. *Nat. Struct. Mol. Biol.* **17**, 1210–1217 (2010).
62. C. J. Fischer, N. K. Maluf, T. M. Lohman, Mechanism of ATP-dependent translocation of *E.coli* UvrD monomers along single-stranded DNA. *J. Mol. Biol.* **344**, 1287–1309 (2004).
63. E. J. Tomko, C. J. Fischer, T. M. Lohman, Single-stranded DNA translocation of *E. coli* UvrD monomer is tightly coupled to ATP hydrolysis. *J. Mol. Biol.* **418**, 32–46 (2012).
64. A. L. Lucius, N. K. Maluf, C. J. Fischer, T. M. Lohman, General methods for analysis of sequential "n-step" kinetic mechanisms: Application to single turnover kinetics of helicase-catalyzed DNA unwinding. *Biophys. J.* **85**, 2224–2239 (2003).
65. H. S. Subramanya, L. E. Bird, J. A. Brannigan, D. B. Wigley, Crystal structure of a DExx box DNA helicase. *Nature* **384**, 379–383 (1996).
66. S. Korolev, J. Hsieh, G. H. Gauss, T. M. Lohman, G. Waksman, Major domain swiveling revealed by the crystal structures of complexes of *E. coli* Rep helicase bound to single-stranded DNA and ADP. *Cell* **90**, 635–647 (1997).
67. S. S. Velankar, P. Soultanas, M. S. Dillingham, H. S. Subramanya, D. B. Wigley, Crystal structures of complexes of PcrA DNA helicase with a DNA substrate indicate an inchworm mechanism. *Cell* **97**, 75–84 (1999).
68. J. Y. Lee, W. Yang, UvrD helicase unwinds DNA one base pair at a time by a two-part power stroke. *Cell* **127**, 1349–1360 (2006).
69. H. Jia *et al.*, Rotations of the 2B sub-domain of *E. coli* UvrD helicase/translocase coupled to nucleotide and DNA binding. *J. Mol. Biol.* **411**, 633–648 (2011).
70. H. Yokota, Y. A. Chujo, Y. Harada, Single-molecule imaging of the oligomer formation of the nonhexameric *Escherichia coli* UvrD helicase. *Biophys. J.* **104**, 924–933 (2013).
71. J. Park *et al.*, PcrA helicase dismantles RecA filaments by reeling in DNA in uniform steps. *Cell* **142**, 544–555 (2010).
72. B. Sun *et al.*, Impediment of *E. coli* UvrD by DNA-destabilizing force reveals a strained-inchworm mechanism of DNA unwinding. *EMBO J.* **27**, 3279–3287 (2008).
73. P. Soultanas, M. S. Dillingham, P. Wiley, M. R. Webb, D. B. Wigley, Uncoupling DNA translocation and helicase activity in PcrA: Direct evidence for an active mechanism. *EMBO J.* **19**, 3799–3810 (2000).
74. M. R. Singleton, M. S. Dillingham, M. Gaudier, S. C. Kowalczykowski, D. B. Wigley, Crystal structure of RecBCD enzyme reveals a machine for processing DNA breaks. *Nature* **432**, 187–193 (2004).
75. M. Wilkinson, Y. Chaban, D. B. Wigley, Mechanism for nuclease regulation in RecBCD. *eLife* **5**, e18227 (2016).
76. B. Nguyen, M. K. Shinn, E. Weiland, T. M. Lohman, Regulation of *E. coli* Rep helicase activity by PriC. *J. Mol. Biol.* **433**, 167072 (2021).
77. P. Singh *et al.*, *Mycobacterium tuberculosis* UvrD1 and UvrA proteins suppress DNA strand exchange promoted by cognate and noncognate RecA proteins. *Biochemistry* **49**, 4872–4883 (2010).

Downloaded at SCHL MED LIB&77680003 on February 16, 2022

78. A. Williams *et al.*, UvrD2 is essential in *Mycobacterium tuberculosis*, but its helicase activity is not required. *J. Bacteriol.* **193**, 4487–4494 (2011).
79. K. H. Darwin, C. F. Nathan, Role for nucleotide excision repair in virulence of *Mycobacterium tuberculosis*. *Infect. Immun.* **73**, 4581–4587 (2005).
80. S. K. Matta, D. Kumar, Hypoxia and classical activation limits *Mycobacterium tuberculosis* survival by Akt-dependent glycolytic shift in macrophages. *Cell Death Discov.* **2**, 16022 (2016).
81. B. Springer *et al.*, Lack of mismatch correction facilitates genome evolution in mycobacteria. *Mol. Microbiol.* **53**, 1601–1609 (2004).
82. L. Cabusora, E. Sutton, A. Fulmer, C. V. Forst, Differential network expression during drug and stress response. *Bioinformatics* **21**, 2898–2905 (2005).
83. C. Güthlein *et al.*, Characterization of the mycobacterial NER system reveals novel functions of the uvrD1 helicase. *J. Bacteriol.* **191**, 555–562 (2009).
84. J. A. Imlay, S. Linn, Mutagenesis and stress responses induced in *Escherichia coli* by hydrogen peroxide. *J. Bacteriol.* **169**, 2967–2976 (1987).
85. L. A. Kelley, S. Mezulis, C. M. Yates, M. N. Wass, M. J. E. Sternberg, The Phyre2 web portal for protein modeling, prediction and analysis. *Nat. Protoc.* **10**, 845–858 (2015).
86. F. Sievers *et al.*, Fast, scalable generation of high-quality protein multiple sequence alignments using Clustal Omega. *Mol. Syst. Biol.* **7**, 539 (2011).
87. G. Perrière, M. Gouy, WWW-query: An on-line retrieval system for biological sequence banks. *Biochimie* **78**, 364–369 (1996).
88. E. Tomko, "Transient-state kinetic studies of *Escherichia coli* UvrD monomer translocation along single-stranded DNA," PhD thesis, Washington University in St. Louis, St. Louis, MO (2010).
89. L. D. Inners, G. Felsenfeld, Conformation of polyribouridylic acid in solution. *J. Mol. Biol.* **50**, 373–389 (1970).
90. J. P. Gabrielson, K. K. Arthur, B. S. Kendrick, T. W. Randolph, M. R. Stoner, Common excipients impair detection of protein aggregates during sedimentation velocity analytical ultracentrifugation. *J. Pharm. Sci.* **98**, 50–62 (2009).
91. T. M. Laue, B. D. Shah, T. M. Ridgeway, S. L. Pelletier, "Computer-aided interpretation of analytical sedimentation data for proteins" in *Analytical Ultracentrifugation in Biochemistry and Polymer Science*, S. Harding, A. Rowe, J. Horton, Eds. (Royal Society of Chemistry, 1992), pp. 90–125.
92. J. Dam, P. Schuck, Calculating sedimentation coefficient distributions by direct modeling of sedimentation velocity concentration profiles. *Methods Enzymol.* **384**, 185–212 (2004).
93. D. P. Mascotti, T. M. Lohman, Thermodynamics of charged oligopeptide-heparin interactions. *Biochemistry* **34**, 2908–2915 (1995).
94. J. R. Lakowicz, "Fluorescence anisotropy" in *Principles of Fluorescence Spectroscopy* (Springer US, 1999), pp. 291–319.

Downloaded at SCHL MED LIB&77680003 on February 16, 2022